

IRMGR44018

Master Thesis

Fabrication of Silicon nanoparticle-Carbon nanofiber anode  
for Li-ion batteries by electrospinning with modification of  
Carbon nanotube and Graphene oxide

Author: Mochan Mishra

Supervisor: Prof. Anna-Lena Kjøniksen



## Acknowledgement

I would like to take this moment to extend my heartfelt thanks to all individuals whose assistance played a pivotal role in the completion of this research. The accomplishment of this task was made achievable through the invaluable contributions of a few skilled and innovative individuals. Foremost, I wish to express my deep appreciation to my supervisor, Anna-Lena Kjøniksen, a Professor in the Department of Engineering at Østfold University College, whose unwavering guidance enriched my scientific acumen. Gratitude is also owed to Susana Garcia Sanfelix, an Associate Professor and course coordinator in the same department, for her insightful advice and collaborative spirit throughout the program. Furthermore, I extend my thankfulness to Cartagena University and the University of Oslo for their assistance in facilitating material characterization tests and performance tests respectively.

## Abstract

Silicon based anodes are being proposed as one of the best options for next generation lithium-ion batteries, however they have certain drawbacks which are preventing their widespread use. In this research a silicon-carbon anode composite is made to mitigate these drawbacks. Silicon nanoparticles-carbon nanofiber 3-D matrix structure is made using electrospinning with further modification of carbon nanotubes and graphene oxide. The fabrication of the anode composite was largely but not entirely successful with partial carbonization. Material characterization and electrochemical testing showed poor results. Anode composite achieved a specific capacity of 10 mAh during first discharge cycle. Columbic efficiency after 200 cycles was 95%.

## Contents

Acknowledgement .....	2
Abstract.....	3
List of figures.....	5
Abbreviations .....	5
Introduction .....	6
Objective .....	12
Experimental .....	13
Materials .....	13
Production of anode material.....	13
Fabrication of working half cells .....	20
Material Characterization .....	22
Results and discussion .....	22
Electrochemical testing.....	26
Conclusion and future work.....	31
References .....	33

## Abbreviations

CE	Columbic efficiency
CNF	Carbon nanofiber
DMC	Dimethyl carbonate
DMF	Dimethyl formaldehyde
EC	Ethylene carbonate
FEC	Fluoroethylene carbonate
FT-IR	Fourier transform infrared spectroscopy
GCD	Galvanostatic charge discharge
GO/rGO	Graphene oxide/reduced graphene oxide
Gr	Graphite
LIBs	Lithium-ion batteries
PAN	Polyacrylonitrile
PANF	Polyacrylonitrile fibres
PP	Polypropylene
SEI	Solid electrolyte interphase
SiNP	Silicon nanoparticles

## Introduction

Clean energy systems like solar and wind have been growing in size and popularity around the world, which has led to a strong demand for efficient storage technologies to properly utilize the energy systems. At the same time, significant efforts have been made to electrify the transport sector to reduce petroleum usage. Lithium-ion batteries (LIBs) have emerged as the major energy storage technology for these applications. Moreover, LIBs are getting increasingly popular in the portable electronic device market. LIBs have found application in wide variety of markets and situations due to their environment friendly potential, relatively high energy density and stable performance. The usage potential and popularity of LIBs as a secondary storage system when compared to other rechargeable batteries, such as nickel metal hydride batteries, and nickel-cadmium is due to higher energy density, higher operating voltages, lower self-discharge potential and lower maintenance [4, 7, 8]. Current commercial LIBs heavily rely on graphite anode which cannot meet the increasing energy density demand, operation reliability and system integration arising from modern applications like smart grids, portable electronic devices, and electric vehicles. The intrinsic specific capacity ( $372 \text{ mA h g}^{-1}$ ) of graphite anodes is low and they exhibit safety concerns due to lithium plating [9]. Hence, research on the next generation anode materials with favourable characteristics like high capacity, good charge/discharge potential, safe operation and low manufacturing costs have attracted great interest in recent years [2].

### Electrochemistry of Lithium-ion Batteries

A lithium-ion battery cell is made up of three primary components, an anode (negative terminal), a cathode (positive terminal), and electrolyte (non-aqueous liquid) which allows the flow of ions between the two electrodes. Another component is the separator which is a porous polymeric film that separates the electrodes while enabling the exchange of lithium ions from one side to the other [10].

The majority of commercial Li-ion batteries employ insertion type electrodes with lithium metal oxides like  $\text{LiCoO}_2$ ,  $\text{LiNiO}_2$ , and  $\text{LiMn}_2\text{O}_4$  as cathodes and carbon materials like graphite as anodes. Anodes and cathodes undergo insertion. The mechanism of the reaction works on the migration of  $\text{Li}^+$  cations being intercalated into and deintercalated out of the cathode and the anode (fig 1). During charge,  $\text{Li}^+$  migrates from the cathode and intercalates into the anode

while travelling through the electrolyte. During discharge, positive electrodes act as the source of lithium ions;  $\text{Li}^+$  migrates from the anode to the cathode. For every  $\text{Li}^+$  released during the reaction, an electron is simultaneously released which then powers the external circuit [4, 11].

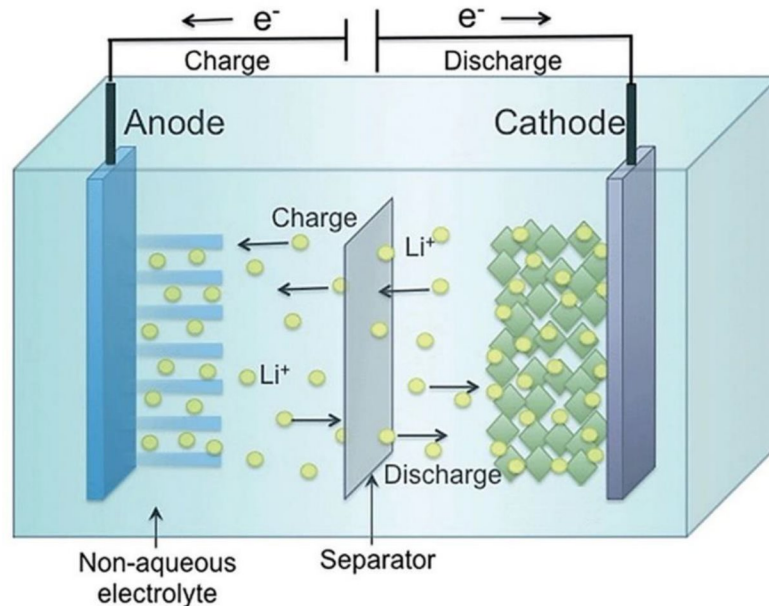
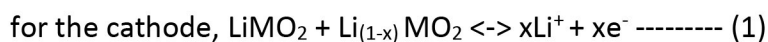


Fig 1. Working mechanism of a lithium-ion battery showing the intercalation of lithium-ions into the anode and cathode upon charge and discharge, respectively. Reprinted from [4].

The half-reactions which are one component of reduction-oxidation reaction for the two electrodes can be written as-



Where, the cathode ( $\text{LiMO}_2$ ) is composed of lithium metal oxides, with M being a transition metal and the anode is graphite. For  $\text{LiMO}_2$ , during charging, the transition metal is oxidized from  $\text{M}^{3+}$  to  $\text{M}^{4+}$  and during discharging, reduced from  $\text{M}^{4+}$  to  $\text{M}^{3+}$  [11]. During initial cyclic reactions, a small amount of the electrolyte undergoes decomposition, which produces a film on the surface of both electrode structures. This film is called solid electrolyte interphase (SEI) and its formation is directly linked to proper functioning and longevity of the battery. Although initially, the SEI layer leads to irreversible loss of capacity in a cell, it crucially acts as a protective layer preventing further decomposition of the electrolyte while allowing for the diffusion of lithium during the discharging and charging processes [4, 11].

### **Initial development of Li-ion Batteries**

The rechargeable battery technologies that were in use before LIB like Ni metal hydride and lead-acid batteries had low energy densities which limited their future potential [12]. In search for a higher energy density system, researchers were drawn to lithium because of its high reducing nature ( $-3.04$  V vs standard hydrogen electrode) and low atomic mass. Theoretically, the small atomic radius of Li-ions gave a high diffusion coefficient when utilized as the charge carrier and appeared to be a very promising solution for the high energy density and high-power requirements of portable energy storage devices [13].

Early development efforts for secondary (rechargeable) lithium batteries were largely unfruitful owing to various reasons. The first commercial implementation of secondary lithium batteries appeared in the late 1970s to early 1980s, using  $\text{TiS}_2$  and  $\text{MoS}_2$  cathodes, and liquid organic electrolytes. However, operational issues, such as fire occurrences, quickly convinced researchers that there were issues preventing the safe and prolonged use of these lithium batteries. The main problem was associated with the Lithium anode. Due to its very high reactivity, lithium metal easily reacts with the electrolyte forming a passivation layer on its surface. The layer is known as solid electrolyte interface (SEI). Extreme cases could result in shorting of the cell [14].

To achieve better cycle life and safety, eventually the replacement of the lithium metal with a less aggressive anode material was identified as the best option. The strategy that was ultimately effective was depending on a brand-new idea that considered the combination of two insertion electrodes, one of which could take lithium ions and function as the anode and the other of which could release lithium ions and function as the cathode. The strategy that was ultimately effective was depending on a brand-new idea that took into account the combination of two insertion electrodes, one of which could take lithium ions and function as the anode and the other of which could release lithium ions and function as the cathode [14]. The electrochemical process of the cell involved the transfer of lithium ions between the two intercalation electrodes. During charging, the anode (negative intercalation electrode) acts as a lithium sink, and cathode (positive electrode) as a lithium source. The process is then reversed upon discharge and cyclically repeated. This concept was first theorized in the late 1970s and practically demonstrated in the early 1980s [15-17].

It would take another 10 years for the concept to reach a practical application when in 1991 Sony demonstrated a battery. The Sony battery featured a proper definition of electrode materials, with graphite as the anode and in lithium cobalt oxide as the cathode [18]. The cathode's function is crucial since it must be able to deliver lithium ions to ensure the electrochemical process and accept them back in a reversible way to ensure the battery's longevity.  $\text{LiCoO}_2$  provided these characteristics successfully. This cathode material was first described in 1980 [19]. This was a fundamental discovery, driving the success of these batteries. The carbon-based anode was found to be the most promising among all the direction of anode research. The success of the carbon anode was due to high reversibility of lithiation/delithiation reactions. Carbon also had good theoretical capacity of  $372 \text{ mAh g}^{-1}$  as well as low lithiation potential. Intercalation based graphite anode was first reported in mid 1970s [14].

### **Silicon Anodes**

At present, the conventional commercial graphite (Gr) anode materials are no longer capable of meeting the requirements for high-performance LIBs due to relatively poor charge holding capacity [20-22]. Silicon has appeared as a material of choice to make high performance anode material because of its reasonable operating potential and natural abundance. The cost of production for both single crystalline and polycrystalline Si has dropped to an acceptable range for electrode applications. It has a very high theoretical capacity of  $4,200 \text{ mAh/g}$  on complete lithiation forming  $\text{Li}_{22}\text{Si}_5$ . Si exhibits appropriately low discharge voltage of  $0.4 \text{ V}$  in average, successfully striking a balance between maintaining a reasonable open circuit voltage and preventing a harmful lithium plating process [23]. Also, Si has other favourable properties, such as good environmental compatibility, relatively stable chemical property, and low toxicity [7].

However, Si has some notable drawbacks in usage (see fig 2). During the lithiation/delithiation process, Si undergoes drastic volume expansion of around 360%, accompanied by large stress generation which has destructive consequences [24]. This results in three major consequences. (1) The structural integrity of the electrode is deteriorated due to pulverization which increases gradually during repeated cyclic processes. (2) Interfacial stress leads to disconnection between electrode and current collector. (3) SEI (solid electrolyte

interface) layer forms, breaks and reforms continuously resulting in consumption of lithium ions. These processes combined instigate an accelerated electrode collapse and capacity fade. Furthermore, Si electrodes have poor electrochemical kinetics due to low intrinsic electron conductivity [23, 25, 26].

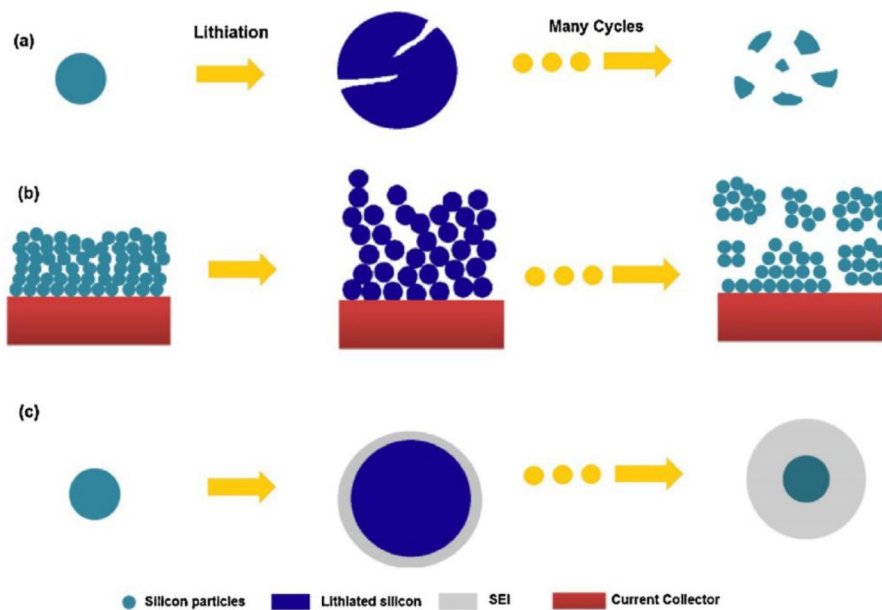


Fig 2. Three distinct Si electrode failure mechanisms, a) electrode pulverization, b) the entire electrode collapsing, and c) The SEI layer is always breaking and growing continuously. Reprinted from [2]

### Mitigating the drawbacks silicon anodes

The obvious benefits of using silicon as anode material have been known for quite a while and multitude of efforts have been made to mitigate the critical drawbacks of Si anodes. Since 1990s, strategies which have been researched are utilizing nanoscale silicon, making composites with buffer design for stress-relief, and accommodating volume expansion with physical compartments. Simply put, the efforts can be classified as two criteria, first is the Si structure, such as 0-D Si nanoparticles, 1-D Si nanowires and 2-D Si thin films. Second criterion is about strategy of modification of Si. This includes different compositions, where Si is combined with carbon composites, metals, metal oxides and other materials, and making hierarchical structures like, yolk-shell, core-shell, embedding, etc. [26].

Si nanostructure has been reported to show good electrochemical characteristics. Multiple articles have reported Si nanotube structures to have shown 80-85% capacity retention after 50-100 cycles at different C-rates. The battery C-rate is a measure of the rate at which a battery's charge or discharge current is expressed in terms of its capacity, where 1C corresponds to a current that charges or discharges the battery in one hour [27, 28]. Although various different Si nanostructures have shown good performance as anodes in lithium-ion batteries, nanostructured Si materials on their own exhibit fast capacity fading, limiting their practical use [23].

The use of Graphene with Si is one viable option, it can improve the performance of the battery by improving the overall charge transportation mechanism [29]. Si/Graphene composites can be fabricated through a few different methods, notably with sonication followed by vacuum-filtration. However, most of the Si/graphene composites were found lacking in cyclic performance. One of the key issues to address using composite anodes is the weak carbon-Si structural interface. Si and carbon are associated with different volume changes during lithium-ion intercalation/de-intercalation. This can trigger rapid delamination, especially at higher charge-discharge rates [23]. CNTs are the most popular 1D carbon material for making composites. When added with Si they can improve the electrochemical properties of the composite. In a reported fabrication of Si-CNT composite as anode for lithium-ion battery, the CNT matrix was shown to accommodate the volume change associated with SiNPs and enabled constant pathways for effective charge transport along the fiber axis. Hence, the electrochemical performance and electronic conductivity of the composite anodes can be enhanced by CNTs [23, 30].

### **SiNPs-Carbon nanofiber composite anodes**

Three-dimensional nano-architectures like carbon nanofiber composites have attracted significant research interest for anodes in Li-ion battery as the structure provides several advantages. Studies have reported significant specific capacity improvement and better cyclic performance when SiNPs are deposited in carbon nanofiber matrix [23].

A 2009 study showed loading of Si nanoparticles in carbon nanofibers resulted in an advanced anode composite which was able to absorb Si volume change effectively and exhibit good electrochemical properties like large reversible capacity and high capacity retention [31]. A

2013 article used CNTs along with SiNPs in a carbon nanofiber matrix prepared by electrospinning and reported that CNTs can further improve conductivity and electrochemical performance. At specific current of  $300 \text{ mA g}^{-1}$ , the Si/CNT/nanofiber anode had 44.3% higher capacity than the anode without CNT after 30 cycles. The Si/CNT/ nanofiber anode also had better rate performance. A 2014 article used electrospinning to make silicon nanoparticle/porous carbon nanofiber composites with high silicon content (52wt.%). The composite exhibited good accommodation for Si volume expansion. Also, the carbon matrix was found to minimize the direct exposure of Silicon to the electrolyte, resulting in better structural stability. The anode had good stable cycling performance of  $870 \text{ mAh g}^{-1}$  at  $0.1 \text{ A g}^{-1}$  after 100 cycles [32]. A 2021 article reported use of graphene oxide along with SiNPs and carbon nano fibres for making composite anodes. Electrospinning was used to make silicon/reduced graphene oxide/carbon nanofibers composite. The Graphene modified layer was made as additional buffer for SiNP volumetric expansion of silicon nanoparticles, and to enhance the electrical conductivity. This composite anode had good cyclic stability and superior rate performance. After 100 cycles, it maintained a specific capacity of  $929 \text{ mA h g}^{-1}$  with 83.1% retention at  $0.5 \text{ A g}^{-1}$ . The rate capability was  $1003 \text{ mA h g}^{-1}$  at  $2 \text{ A g}^{-1}$  [33]. All the composite anodes with 3-D carbon nano fibres require stabilization and carbonization at moderately high and high temperatures respectively to attain the carbon fibre matrix and stable structure.

## Objective

The primary objective of the research is exploring a method to fabricate SiNP-CNF composite anodes with focus on simplicity and using minimal specialized equipment. The procedure should be a replicable process which can be reliably followed in a lab. Second objective is to successfully incorporate a triple modification in the composite fibre with SiNP, CNT and GO with the possibility of making mass percentage adjustments to each modifier. Third objective is to successfully test and characterize the anode material to find out material structure and electrochemical performance.

## Experimental

### Materials

Silicon powder (crystalline, APS  $\leq 50$ nm, thermo scientific), carbon nanotube (multi-walled, 50-100 nm diameter,  $>5\mu\text{m}$  length, Tokyo chemical industry co., ltd.) and graphene oxide powder (powder, 15-20 sheets, 4-10% edge oxidized, Sigma-Aldrich) were used in the first part of the fabrication. Polyacrylonitrile (molar mass 53.06 g/mol), Pluronic F-127 (poly(ethylene oxide)<sub>20</sub>-*b*-poly(propylene oxide)<sub>70</sub>-*b*-poly(ethylene oxide)<sub>20</sub>) and dimethyl formaldehyde were used in the second part of the fabrication. Lithium hexafluorophosphate solution in ethylene carbonate and dimethyl carbonate (Sigma-Aldrich), fluoroethylene carbonate (Sigma-Aldrich) were used in cell assembly.

### Production of anode material

The anode is a SiNPs-carbon nanofiber composite anode with addition of graphene oxide (GO) and carbon nanotubes (CNTs) to the composite matrix. The finished anode has a complex structure which can withstand volumetric change of SiNPs and exhibit excellent electrochemical properties. The process of anode fabrication is divided in three parts. The first part includes a sequence of procedures which gives us a homogenous mixture of SiNPs and carbon nanotubes with graphene oxide and is labelled as SiNP/CNT/GO. The second part includes a sequence of procedures which combines the polyacrylonitrile fibres (PANF) with the SiNP/CNT/GO mixture in a way that the mixture is homogeneously loaded in PANF. The resulting fibrous material is labelled as SiNP/CNT/GO@PANF. The third part includes the stabilization and carbonization of SiNP/CNT/GO@PANF to convert polyacrylonitrile fibres (PANF) to carbon nano fibres (CNF) and reduce the graphene oxide to get the anode composite which is labelled as SiNP/CNT/rGO@CNF.

#### 1. Preparation of SiNP/CNT/GO

First, a homogenous suspension of SiNPs and CNTs was obtained. 1g silicon powder and 0.3g carbon is mixed in 100ml absolute ethanol. This mixture is then ultrasonicated for 1h on a Qsonica Q500 ultrasonicator at 20% amplitude to obtain a homogenous suspension of SiNP-CNT (fig 3). Sonication is a process that involves using high-frequency sound waves

(ultrasound) to agitate and disrupt particles, cells, or materials in a liquid medium. It is commonly used in various scientific and industrial applications, including sample preparation and dispersion of nanoparticles [34]. The graphene oxide dispersion was obtained by mixing



*Fig 3. Ultrasonication of SiNPs and CNTs*



*Fig 4. Bath ultrasonication GO*

0.1g of graphene oxide powder with 50 ml deionized water and dispersing the graphene oxide with a cold-water bath ultrasonication on an Elma Schmidbauer ultrasonicator (45 kHz, 85% amplitude) (fig 4).

The SiNP-CNT homogenous suspension is then mixed with GO solution while under magnetic stirring. The new SiNP-CNT-GO suspension is then left in a temperature-controlled oven at



*Fig 6. The SiNP-CNT-GO suspension in the oven on a magnetic stirrer.*



*Fig 5. SiNP/CNT/GO*

80°C while being continuously stirred using magnetic stirring (fig 5). This evaporates all the liquid leaving only a powdered mixture behind which is SiNP/CNT/GO (fig 6).

## **2. Preparation of SiNP/CNT/GO@PANF**

The previously obtained SiNP/CNT/GO was mixed with polyacrylonitrile (PAN) and Pluronic F-127 in dimethyl formaldehyde (DMF) to get a homogenous viscous solution. PAN dissolved in DMF has been widely used to make nanofibers. The PAN fibres are the precursor to carbon nanofibers (CNF) [35]. Pluronic F-127 is used as a dispersant to evenly disperse SiNPs in the SiNP/CNT/GO-PAN-DMF liquid solution. The use of dispersants to avoid coagulation of SiNPs and as a result enhance performance has been reported before. Wang et al. [32] used F-127 to make a uniform silicon nanoparticle/porous carbon nanofibers free standing anode for lithium batteries. The use of dispersant enabled uniform distribution of SiNPs in the polymer fibres and was associated with improved cyclic stability. Yan et al. [33] reported the use of P123 to make SiNP-Carbon nanofiber anode with dual modification.

0.92g of SiNP/CNT/GO, 1.46g of PAN and 0.7g of P127 was mixed in 20ml of DMF. The mixture was magnetically stirred at 60 °C for 8 hours in a temperature-controlled chamber. The resulting viscous liquid is used for electrospinning. Electrospinning is a nanofabrication technique used to produce ultrafine fibres ranging from tens of nanometres to a few micrometres in diameter. It involves the use of an electric field to draw a charged polymer solution into an extremely thin fibre, which solidifies upon collection [36].

Electrospinning is a popular method to fabricate PAN nanofibers. Electrospinning of PAN to make nanofibers followed by stabilization and carbonization to fabricate carbon nanofibers is a very well reported and understood process [35, 37]. Electrospinning of the viscous solution was done in a vertical orientation on Bioinicia Spinbox bench-top electrospinning machine. The liquid was dispensed from a plastic syringe through a thin tube with a blunt metal needle connected to the end. The electrospinning parameters are noted in table 1. The resulting nanofibers were collected on aluminium foil (flat plane collector) as shown in figure 7 (a) and (b) labelled as SiNP/CNT/GO@PANF.

Table 1. Electrospinning parameters

Spinning distance	12.0 cm
Vertical distance	11.6 cm
Feed rate	0.5 ml/h
Total feed volume	15.0 ml
Electric field	17.0 kV
Needle	1.20 x 40 mm (dia. x length)

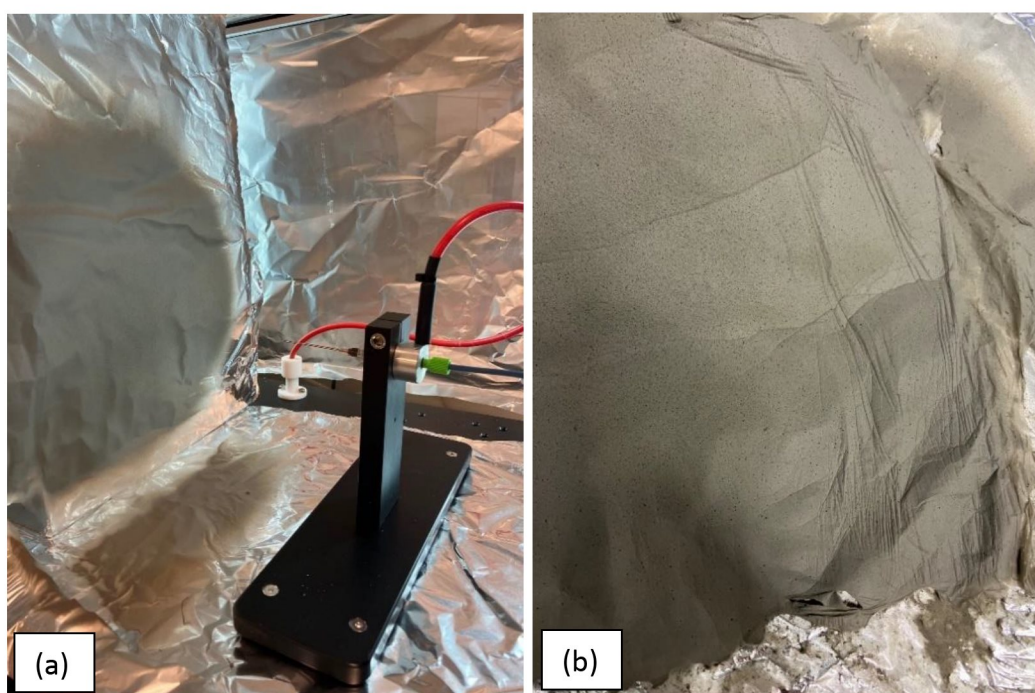


Fig 7. (a) Electrospinning of PAN fibres (b) Collected PAN nanofibers

### 3. Preparation of SiNP/CNT/rGO@CNF

Collected nanofibers on the previous step labelled as SiNP/CNT/GO@PANF are treated using a 2-step procedure of firstly stabilization and then carbonization. This is a well understood procedure to convert polyacrylonitrile (PAN) nanofibers into carbon nanofibers. Stabilization is a crucial stage in transforming PAN fibres into high-performance carbon fibres. During stabilization, the precursor fibres are exposed to temperatures between 200 to 300 °C for over an hour in the presence of air [38, 39]. This process leads to significant changes in the fibres' chemical structure, imparting them with thermal stability. As a result of various

reactions, such as cyclization, dehydrogenation, aromatization, oxidation, and crosslinking, the triple bond ( $C\equiv N$ ) in PAN is converted into a double bond ( $C=N$ ). Consequently, the linear PAN chains are transformed into cyclic or ladder-like structures, ensuring the fibres' thermal stability and preventing melting during subsequent carbonization [39].

Conventionally, following stabilization, the PAN fibres undergo carbonization at temperatures ranging from 800 to 1500 °C in an inert atmosphere, often using nitrogen ( $N_2$ ) or argon (Ar) gases [40]. Carbonization serves to eliminate non-carbon elements in the form of different gases. During this process, the fibre diameters shrink, and the fibres experience a weight loss of approximately 50%. It is important to note that a continuous flow of inert gas is used to eliminate additional gases and non-carbon elements emitted during the procedure [6, 41].

For this research, the stabilization procedure was carried out by placing the fibres in an oven at room temperature and the temperature was gradually increased at the rate of 1 °C per minute until it reached 270 °C at which point the fibres were kept at 270 °C for 1 h. The gradual increase of temperature is important to make sure that fibres do not experience thermal shock which could be detrimental to the structure. It is to be noted that some unwanted changes to the structure of the composite fibres could happen, notably unwanted reactions of silicon nanoparticles are possible at these temperatures to form  $SiO_2$ . A rectangular piece of fibre was cut before stabilization as a control specimen to see the effect of stabilization on the weight of the fibres. The fibres' weight decreased by 20.5% after stabilization. The stabilized fibre can be seen in fig 8.



*Fig 8. Stabilized composite fibre*

The carbonization procedure undertaken was significantly different from the conventional process. Normally, specialised cylindrical quartz chamber is used to place the electrode material with opening on both sides to facilitate constant flow of inert gas. This quartz chamber is kept inside a specialised oven to achieve high temperatures of over 800 °C for several hours. A basic schematic of this is shown in fig 9.

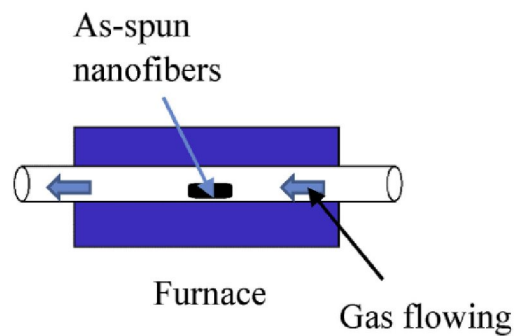


Fig 9. Basic schematic of a typical carbonization process. Reprinted from [5]

However, for this research an alternate technique was devised to explore a simpler and more cost-effective way and due to the lack of specialised carbonization equipment. A boron glass flask with a single valve head was used. The fibres were placed inside the glass flask and the flask was then flushed alternatively with vacuum and argon gas to eliminate as much air as possible as seen in fig. 10&11. The glass head was then closed. The glass flask was then put inside a temperature-controlled oven at room temperature and the temperature was increased at the rate of 3 °C per minute until it reached 500 °C at which point it was held at 500 °C for 1 h. The carbonization process was different in several ways. Firstly, it was not possible to make sure that all air had been eliminated from the glass flask. There was no constant flow of Ar to eliminate all the unwanted gases from the carbonization chamber. The carbonization process itself was restricted to 1 h as carbonization times of longer than 1.5 h resulted in a significantly degraded product. The temperature of carbonization was kept at 500 °C instead of 800 °C and above because the glass flask could not endure higher temperatures.



*Fig 10. Glass flask with electrode material inside (wrapped in a film of copper)*



*Fig 11. Setup to flush the glass flask with vacuum and argon.*

The carbonization process also reduces the graphene oxide (GO) converting it to reduced graphene oxide (rGO). The resulting carbonised fibre was labelled as SiNP/CNT/rGO@CNF and can be seen in fig 12. After carbonization, fibre's weight further decreased by 11.3%.



*Fig 12. Carbonized composite fibre*

## Fabrication of working half cells

### 1. Mass loading and electrode preparation

Mass loading refers to how much mass of each electrode should be present in the working half-cell based on the theoretical capacity calculations. Since the reference electrode is the anode, hence, the theoretical capacity of the counter electrode (cathode) should be larger than that of the presumed theoretical capacity of the anode. For half cells, lithium discs were used as the cathode (fig 13). Lithium discs were 16mm in diameter, 1mm thick with a density of  $0.534 \text{ g/cm}^3$ . Anode half-cells are constructed for testing anode parameters in specific. In anode half-cell, reaction at anode is of concern for the electrochemical properties. In this configuration, lithium metal is used as the counter electrode because it does not introduce any extra cathode specific reactions. This configuration is preferred for testing anode parameters specifically because in a full cell both anodic and cathodic reactions are required to be studied and electrochemical performance is determined by relation between reactions of both electrodes [42, 43]. In case of lithium half cells with silicon-carbon composite anode, the acceptable range for the anode mass loading is around  $1\text{-}5 \text{ mg/cm}^2$  [44]. For this research, freestanding anodes of 10mm diameter were punched from SiNP/CNT/rGO@CNF sheets (fig 14). Since electrospun fibre sheets had different thickness at different points, a range of thickness was seen in final electrodes as well. The thickness of the electrodes used was in the range of  $0.23\text{-}0.37 \text{ mm}$  with the weight of  $1.50\text{-}2.96 \text{ mg}$ . This equates to a mass loading range of  $1.91\text{-}3.77 \text{ mg/cm}^2$ .

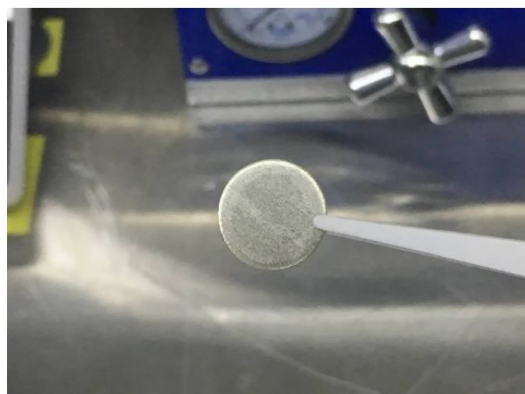


Fig 14. 16mm Li disc as cathode



Fig 13. 10mm anodes punched from the fibre sheets.

## 2. Cell assembly

Cells are assembled using the reference electrode and the counter electrode in a CR2032 cell assembly (Xiamen TOB new energy technology). The electrolyte used was lithium hexafluorophosphate solution in ethylene carbonate and dimethyl with 5% fluoroethylene carbonate added by volume (1.0 M LiPF<sub>6</sub> in EC/DMC 1:1 + 5% FEC). The separator used was 25um polypropylene separator cut into 20mm diameter film (Xiamen TOB new energy technology). The cell assembly took place in a glove box (fig 15&16) with the upside down method, where the assembly starts from the negative side (small casing) on bottom and finishes with the positive side on top (larger casing) (fig 17).



Fig 15. Glove box



Fig 16. Working inside the glove box.

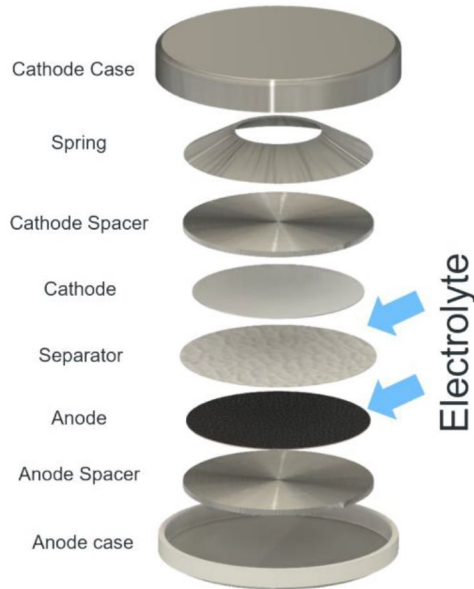


Fig 17. Schematic of cell assembly, reprinted from [1]

## Material Characterization

Material characterization was done by performing Raman Spectroscopy and Fourier Transform Infrared Spectroscopy (FT-IR). These tests were performed on the anode composite SiNP/CNT/rGO@CNF. Raman spectroscopy is a non-destructive analytical technique used to investigate vibrational, rotational, and other low-frequency modes of molecules. For our purposes, Raman spectroscopy can reveal information on molecular bonds present in the composite, which are then analysed to determine whether or not desirable molecular bonding and structure is present in the composite [45]. FT-IR is also used to study molecular vibrations in various types of samples. It can provide valuable information about the chemical composition, molecular structure, and bonding of a sample. For this research, determining chemical composition is primary purpose of employing this technique [46, 47].

## Results and discussion

### Raman spectroscopy

Results of Raman spectroscopy from a similar previous study are shared as reference along with the results from this study. Fig 18 shows the Raman spectra of both stabilized and carbonized composites. Fig 19 shows the reference Raman spectra of a carbon-silicon composite. The sharp peak at  $512\text{ cm}^{-1}$  correspond to the stretching of Si-Si bonds.

Amorphous carbon is indicated by the presence of the D-band (representing disorder) at 1355  $\text{cm}^{-1}$  and the G-band (indicative of graphitic structures) at 1597  $\text{cm}^{-1}$ , both these bands confirmed the presence of CNTs and GO in the composite. A small peak at 957  $\text{cm}^{-1}$  was due to the stretching mode of amorphous Si-Si [28, 48]. The detection of peaks related to both silicon and carbon indicated to the successful creation of the Si-C composite. The ratio of integrated intensities between the D and G bands for the Si-C composite samples is supposed to decrease after successful carbonization. In the reference graph, the decline in the D/G ratio as temperature increases in the graph implies an augmentation in the graphitic quality as the temperature rises. As a result, this enhances the conductivity of the electrode material [3, 49].

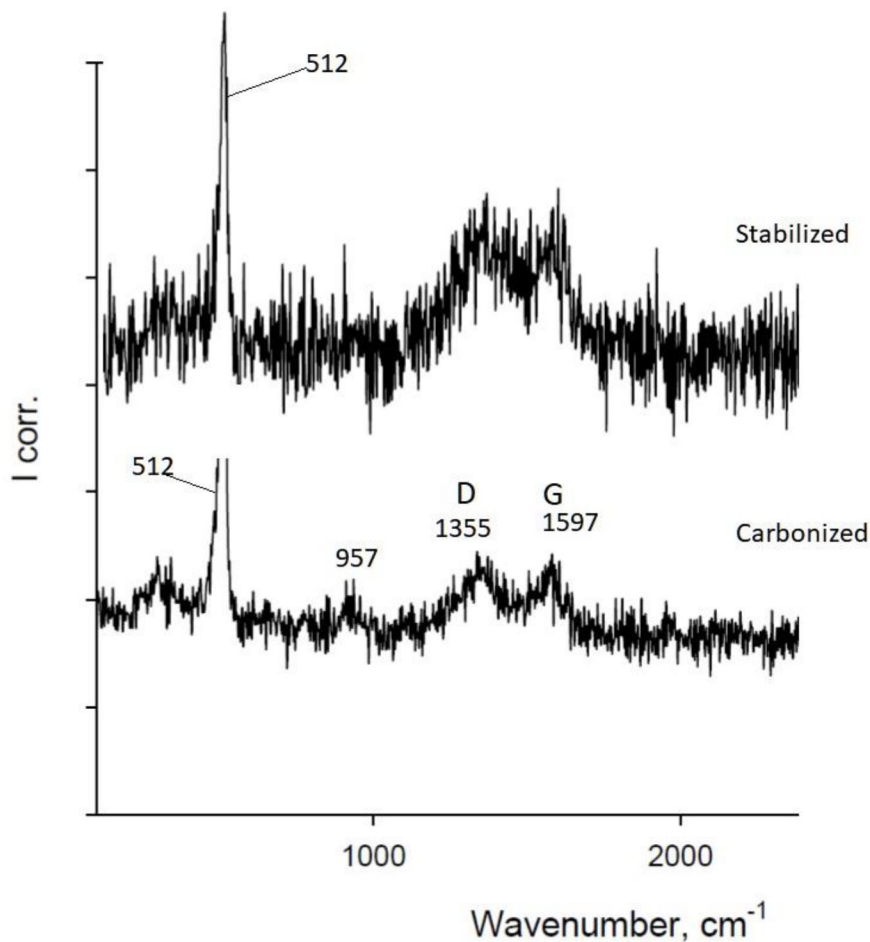


Fig 18. Raman spectroscopy on stabilized and carbonized composite.

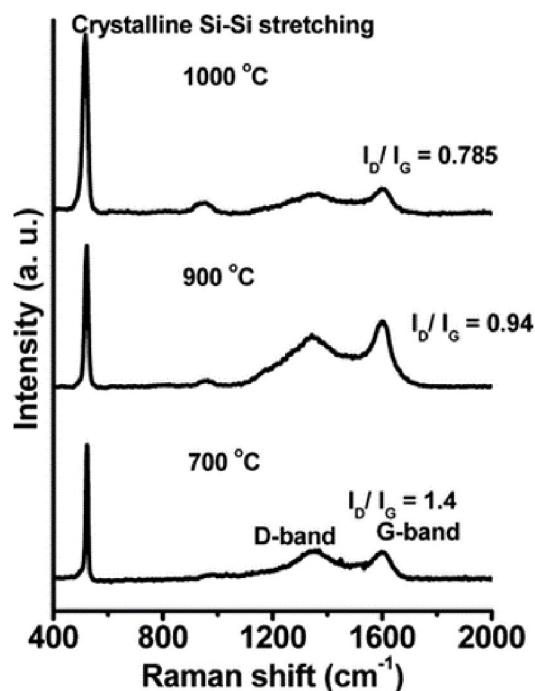


Fig. 19. Raman spectroscopy (for reference) on a carbon-silicon anode. Reprinted from [3]

#### Fourier Transform Infrared Spectroscopy (FT-IR)

FT-IR was done on the carbonized composite. The results of the FT-IR are presented as a graph in fig 20. For reference FT-IR of carbonized PAN nanofibers at different temperatures is shown in fig 21. In fig 20 The characteristic bands at 1065 and 800  $\text{cm}^{-1}$  correspond to the stretching and bending of Si-O bonds, respectively. The arrangement and form of the primary Si-O vibrational peak at 1065  $\text{cm}^{-1}$  indicate a silicon dioxide structure [50]. The small peaks at 1718 and 1556  $\text{cm}^{-1}$  suggest presence of graphitic structures of carbon which can be associated with CNTs and rGO. A range of peaks between 2157 and 2361  $\text{cm}^{-1}$  are associated with CNTs as found out by FT-IR analysis on CNTs done during the research. The carbonyl group indicated at 3448  $\text{cm}^{-1}$  is associated with the stretching vibration of O-H in the C-OH groups, indicating the presence of water content in the composite [51, 52].

The peaks found at 2890–2990  $\text{cm}^{-1}$ , 1390  $\text{cm}^{-1}$ , and 1228  $\text{cm}^{-1}$  correspond to the vibrations of aliphatic CH groups (CH, CH<sub>2</sub>, and CH<sub>3</sub>). In fig 21, as the temperature of carbonization rises, the strength of the peak originating from CH<sub>2</sub> at 2921 and 2851  $\text{cm}^{-1}$  diminishes. It is important to note that this suggests lack of these particular peaks (2890-2990  $\text{cm}^{-1}$ ) suggests complete carbonization of PAN fibres, causing the hydrocarbons to transform into a graphitic structure [6, 53, 54].

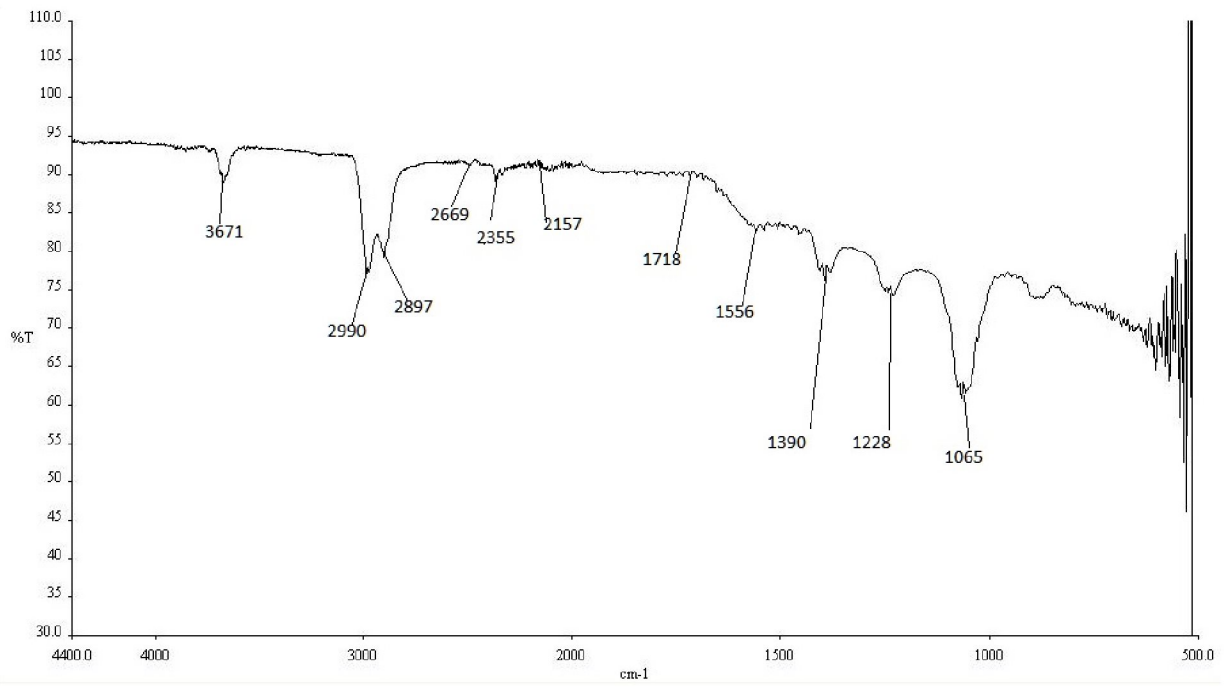


Fig 20. FT-IR of the carbonized composite

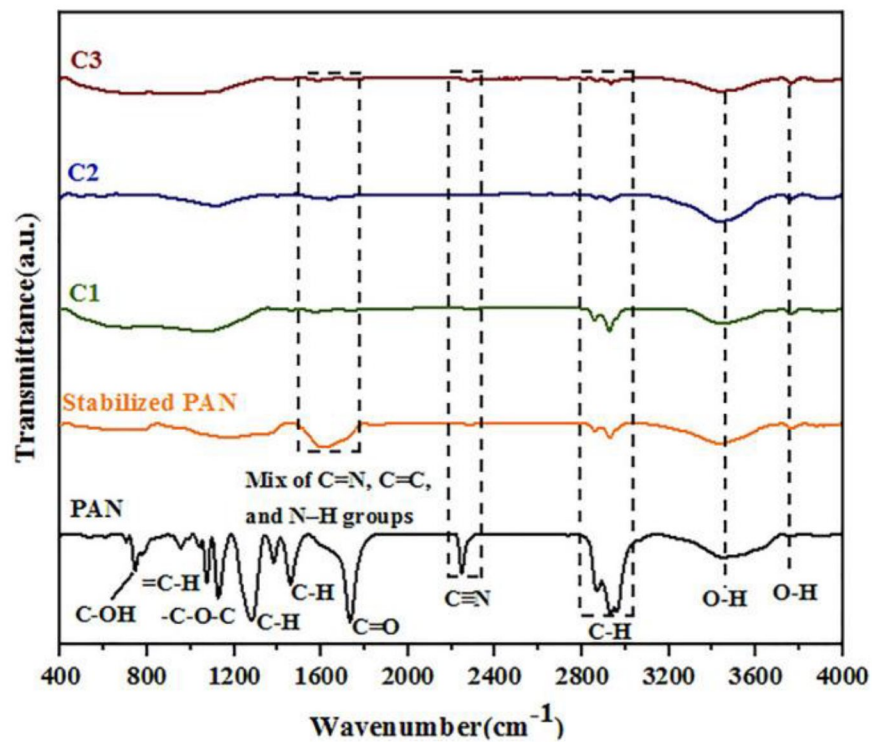


Fig 21. FT-IR of PAN fibres (for reference) at 1000, 1200, and 1400 °C, denoted as C1, C2, C3, respectively. Reprinted from [6]

## Electrochemical testing

The assembled CR2032 cells underwent electrochemical testing to calculate key performance parameters. The testing method used was Galvanostatic Charge-Discharge (GCD). Galvanostatic charge-discharge experiments involve observing the voltage reaction while applying a constant current. This method is highly effective for evaluating the capacity, reversibility, stability of electrode materials. The goal of GCD testing is to gather information about the battery's capacity, voltage profiles, energy efficiency, and other electrochemical characteristics under specific current conditions. During charging phase, a constant current is applied to the battery via an external circuit. This means that a steady flow of electrons is introduced into the battery, causing lithium ions to migrate from one electrode (cathode) to the other electrode (anode) through the electrolyte. During charging, the voltage across the battery increases gradually. During discharging phase, the current direction is reversed, and the battery is discharged at the same constant current. During discharging, the voltage across the battery gradually decreases as the stored energy is released and the lithium ions move back from the anode to the cathode through the electrolyte. By monitoring the voltage and time during both the charge and discharge phases, valuable information about the battery's behaviour can be obtained. Important parameters calculated and studied in this research are capacity-voltage profiles, cyclic performance and coulombic efficiency [55, 56].

GCD measurement requires a constant current value and terminal voltage, at which the current direction will be inverted. A typical single discharge–charge cycle, with an applied current is shown in Fig a. A typical voltage-capacity profile is shown in fig b, where  $E_1$  and  $E_2$  are terminal voltage,  $E_c$  is anode peak voltage and  $E_d$  is cathode peak voltage. It appears as an oblique line with a roughly recognizable plateau. For anode materials that act as acceptors of charge carriers, Coulombic Efficiency (CE) denotes the proportion to which inserted charge carriers can be effectively extracted and can be expressed as a percentage of charge to discharge capacity. This measurement is linked to the relationship between the capacity for charging and discharging. Given the finite quantity of charge carriers present within batteries, any reduction due to factors like electrolyte decomposition typically cannot be regained. As a result, CE plays a crucial role in evaluating the longevity of batteries concerning their sustained charging capability. Cyclic performance is the observation of change in charge

capacity and discharge capacity over number of cycles. The present practice in measuring GCD typically involves standardizing the current with respect to the active material's mass or the electrode's surface area. This choice depends on whether the focus is on gravimetric capacity or areal capacity. In half-cell experiments, the gravimetric capacity (measured in mAh per gram) is frequently employed and was used for this research. The current is adjusted to a specific current value (expressed in units of mA/g) [57, 58].

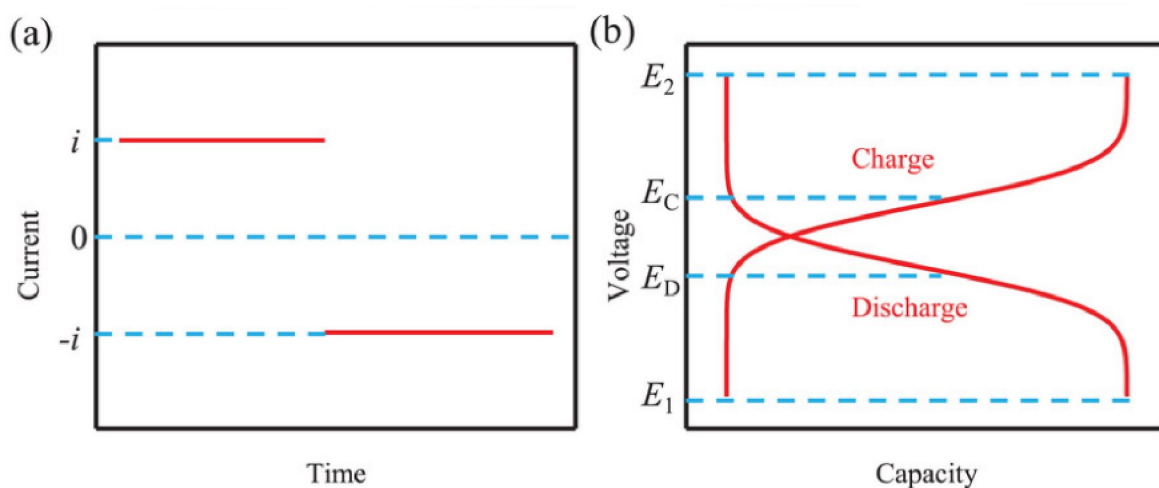


Fig 22. (a) Current profile for charge-discharge, (b) typical voltage vs capacity curve, reprinted from [57].

GCD testing was done on Neware CT-4008T-5V10mA-164 battery testing system designed to measure coin cell electrochemical data. The upper and lower terminal voltage was set as 2 V and 0.05 V. The applied specific current was 100 mA/mg. The electrochemical data is then plot as graphs. In fig 23, the specific capacity-voltage profiles reveal the typical charge discharge curves. The initial discharge capacity was 10.3 mAh while the initial charge capacity was 1.4 mAh. In fig 23, The disparity between initial discharge capacity and the initial charge capacity is the irreversible loss. From looking at the charge-discharge profiles it can be deduced that the cycling window for the GCD test was not precise enough and hence resulted in incomplete charge cycles for almost entirety of the test duration. The initial coulombic efficiency was 14%. In fig 24, coulombic efficiency of the second cycle was 51% and it gradually increased to 94% by the 200<sup>th</sup> cycle. Similarly, in fig 25, the charge capacity cyclic performance also increased over the lifetime, initially it was 1.4 mAh with a considerable difference between it and discharge capacity but they even out by the end of the test to a value of 3.5

mAh. Compared to similar anodes from other research, the initial CE was considerably lower. CE becomes comparable to other research after 200 cycles. Initial specific capacity (both charge and discharge) as well as specific capacity throughout the life of the anode was found to be a mere fraction of what similar anodes have achieved [24, 30, 33].

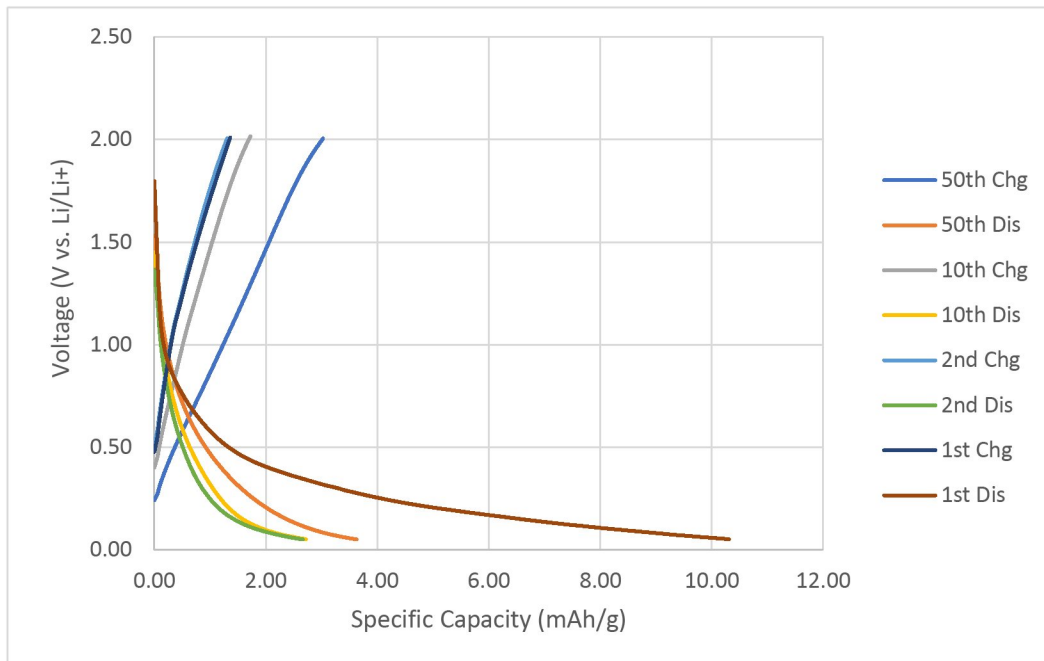


Fig 24. Voltage vs Specific Capacity curves

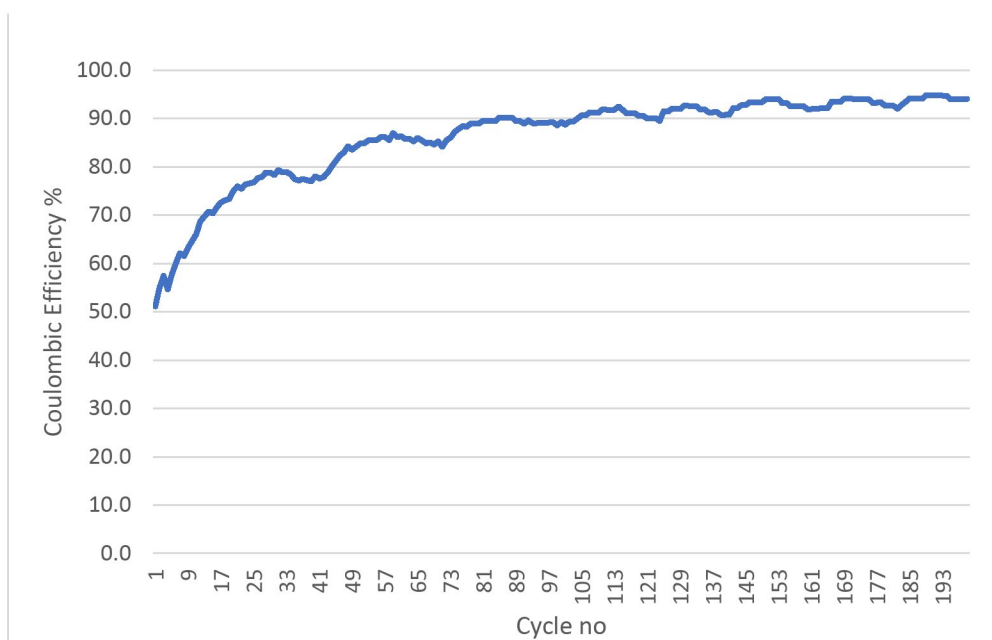


Fig 23. Coulombic efficiency vs cycle number

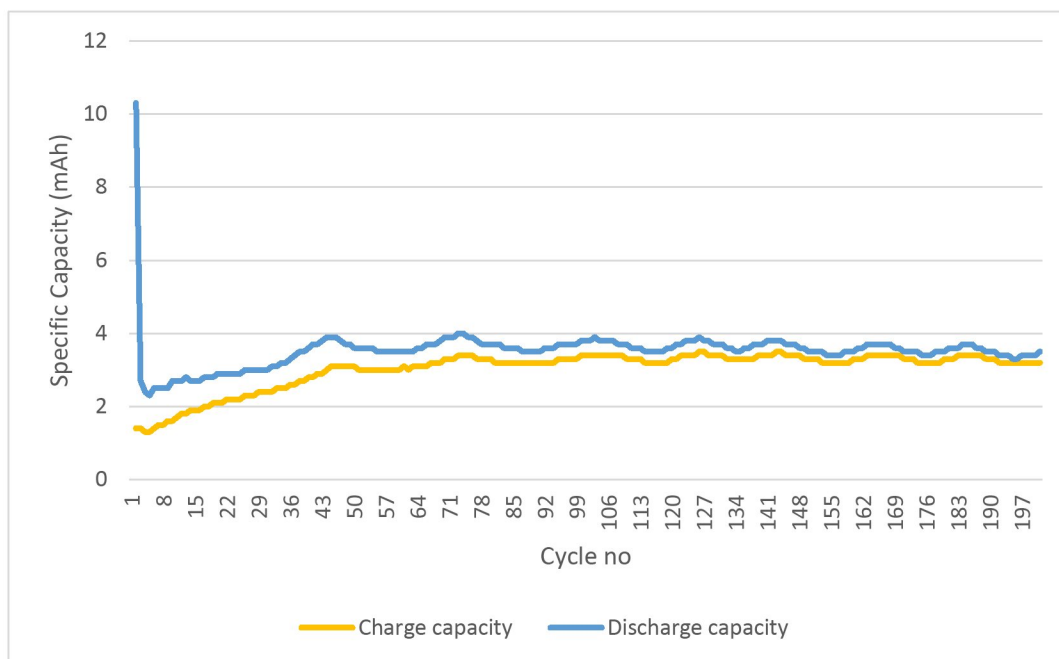


Fig 25. Specific Capacity vs Cycle number

The composite anode cells achieved a first cycle discharge specific capacity of 10.3 mAh and a first cycle charge capacity of 1.4 mAh. The formation of SEI layer results in permanent loss of charge during the first discharge cycle. Although, this does not sufficiently explain the large difference between the first discharge and charge cycle capacity. Looking at the capacity-voltage profiles it can be understood that the voltage cycling range for the GCD testing was the optimum for charge cycles. This resulted in partially incomplete charge cycles exaggerating the difference between first cycle discharge and charge capacities. As the cycle number increases more and more of cycling data for charging enters the voltage range increasing the charge specific capacity. Towards the end of the cyclic testing, charge and discharge capacities are even and show an expected behaviour. The anode sustained a discharge capacity of 3.5 mAh and a columbic efficiency of 95% after 200 cycles. Hence, it can be concluded that the cyclic performance and columbic efficiency of the anode is fairly typical of this kind of anode [59]. However, it is obvious that the anode exhibited a very poor specific capacity throughout the cycling. The specific capacity expected was much larger hence a further look into material structure and fabrication process is required to understand the reason behind the poor electrochemical performance.

FT-IR analysis results provide crucial evidence about unexpected material structure. In FT-IR analysis (fig. 20) the vibrational peak at  $1065\text{ cm}^{-1}$  confirms significant presence silicon dioxide which is highly unwanted for the material structure. The peak at  $3448\text{ cm}^{-1}$  indicates the presence of water content in the composite which is also not expected in a carbonized CNF sample. However, the most important indication of poor carbonization are the peaks found at  $2890\text{--}2990\text{ cm}^{-1}$ . From the reference FT-IR graph (fig. 21) it is understood that these peaks are important indication of complete carbonization of PAN nanofibers. As nanofibers undergo carbonization these peaks are significantly diminished. Moreover, they continue to diminish as the temperature of carbonization rises, causing the hydrocarbons to transform into a graphitic structure. In fig 20, the peaks at  $2890\text{--}2990\text{ cm}^{-1}$  are still very much prominent confirming the incomplete carbonization of PAN nanofibers in the anode composite. It can be understood that the combination of significant presence of  $\text{SiO}_2$  as well as incomplete carbonization of PAN fibres result in extremely poor electrical conductivity and charge holding capacity. Moreover, since the SiNPs and CNTs are embedded in the fibre structure, poor conductivity restricts the electrical pathways to these elements resulting in even worse performance than what would be expected from these elements alone even without the fibre structure. In Raman analysis (fig 18) the ratio of integrated intensities between the D and G bands for the Si-C composite is supposed to decrease after successful carbonization. The decline in the D/G ratio as temperature increases implies an increase in the graphitic nature and conductivity of the material as the temperature rises. However, visually analysing, no noticeable decrease in the D/G ratio is observed between the stabilized and the carbonized material. This indicates that the graphitic nature of the material did not increase as it was expected. To understand the poor material structure fabrication process is required to be examined.

As it is already explained, the carbonization/calcination process used in this research differs significantly from the conventional process. The maximum carbonization temperature achieved was  $500^\circ\text{C}$  which is significantly less than well reported figure of suggested  $800\text{--}1200^\circ\text{C}$  for PAN fibres and  $800\text{--}900^\circ\text{C}$  for Si-CNF composites. The carbonization time at maximum temperature was only 1 h instead of suggested 3-4 h. These factors in combination resulted in partial carbonization. Conventional procedure of carbonization uses a constant

flow of inert gas through the chamber to eliminate gases released during the process. This procedure used a glass flask with inert gas inside it. Presence of air was kept to a minimum, but it was still present. Exhaust gases from the process had no reliable mechanism to escape the chamber. This resulted in formation of  $\text{SiO}_2$  and might have altered the material structure in other ways through interaction with exhaust gases. It can be deduced that the inadequacies in the carbonization/calcination procedure caused poor material structure and electrochemical performance.

## Conclusion and future work

The primary objective of the research was to explore an anode chemistry for SiNP-CNF composite anodes that can be fabricated easily with minimal specialized equipment and have a replicable process which can be reliably followed in a lab. Second objective was to successfully incorporate a triple modification in the composite fibre with the possibility of making mass percentage adjustments to each modifier. Third objective was to successfully test and characterize the anode material with expectation of good electrochemical performance.

The research led to a successful fabrication of a triple modification composite fibre SiNP/CNT/GO@PANF. The fabrication process of composite fibre was largely devoid of complicated machinery and procedures apart from the use of electrospinning machine. The fabrication of SiNP/CNT/GO@PANF was done in a simple to follow and replicable 2 steps as explained in part 1 and 2 of section 'construction of anode material'. These steps provide large control over customizing the quantities of modifiers, SiNP, CNT, and GO. Different mass percentage of SiNPs can be tried to explore and study effects of SiNP on overall anode performance. The fabrication process can also be used as a template to experiment with other composite anode chemistries with CNFs. Through trial and error, an optimum viscosity for precursor homogeneous mixture liquid to electrospinning along with optimum electrospinning parameters were also devised, which can be helpful for anyone further exploring this process or working on similar anode chemistry. However, the third step of fabrication process to make SiNP/CNT/rGO@CNF was found to have various shortcomings. The carbonization temperature was too low and there was no flow of inert gas in the

chamber. These shortcomings led to unwanted material structure and poor electrochemical performance.

Unfortunately, the research did not lead to the fabrication of a completed working anode with good electrochemical performance as described in the primary objective, hence, primary objective was only partially achieved. The second objective was completely achieved as composite fibre had a successful triple modification. The third objective was also only partially achieved as tests were successfully done to determine material structure and to test electrochemical performance but results for both tests were very poor.

The future for silicon-based anodes is extremely promising and SiNP-CNF composite based anodes have enormous potential. There is a lot of ongoing research in this area, and it is expected to continue in the near future. There is no reason to believe that the composite anode material SiNP/CNT/rGO@CNF is not a viable option for next-generation li-ion batteries. As discussed above the poor performance of the composite in this research is due to the inadequate carbonization procedure and the performance ceiling of this composite material as anode is expected to be very high. The research can be continued with a complete revision of carbonization procedure by making necessary adjustments to eliminate the problems discussed above. Any future work should also include different mass percentage concentrations of SiNPs in the composite and their effect on material and electrochemical performance of the anode. Mass percentage of CNT and GO could also be changed for exploring best possible balance between theoretical capacity and electrical conductivity. GCD testing procedure and voltage window for the tests are also required to be explored further to find the best voltage testing window for the anode composite. Energy dispersive X-Ray (EDX) analysis and Scanning Electron Microscopy (SEM) imaging were also done on the anode composite during the research, but their results did not arrive in time to publish in the thesis. EDX and SEM can reveal crucial information about the material structure and any future work is encouraged to employ these techniques.

## References

- [1] B. Zhang, L. Merker, A. Sanin, H.S. Stein, Robotic cell assembly to accelerate battery research, *Digital Discovery* 1(6) (2022) 755-762.
- [2] K.M. Abraham, Prospects and Limits of Energy Storage in Batteries, *The Journal of Physical Chemistry Letters* 6(5) (2015) 830-844.
- [3] S.K. Kumar, S. Ghosh, S.K. Malladi, J. Nanda, S.K. Martha, Nanostructured Silicon–Carbon 3D Electrode Architectures for High-Performance Lithium-Ion Batteries, *ACS Omega* 3(8) (2018) 9598-9606.
- [4] P. Roy, S.K. Srivastava, Nanostructured anode materials for lithium ion batteries, *Journal of Materials Chemistry A* 3(6) (2015) 2454-2484.
- [5] O. Pech, S. Maensiri, Electrochemical performances of electrospun carbon nanofibers, interconnected carbon nanofibers, and carbon-manganese oxide composite nanofibers, *Journal of Alloys and Compounds* 781 (2019) 541-552.
- [6] R. Shokrani Havigh, H. Mahmoudi Chenari, A comprehensive study on the effect of carbonization temperature on the physical and chemical properties of carbon fibers, *Sci Rep* 12(1) (2022) 10704.
- [7] K. Feng, M. Li, W. Liu, A.G. Kashkooli, X. Xiao, M. Cai, Z. Chen, Silicon-Based Anodes for Lithium-Ion Batteries: From Fundamentals to Practical Applications, *Small* 14(8) (2018) 1702737.
- [8] B. Scrosati, J. Garche, Lithium batteries: Status, prospects and future, *Journal of Power Sources* 195(9) (2010) 2419-2430.
- [9] W.-J. Zhang, A review of the electrochemical performance of alloy anodes for lithium-ion batteries, *Journal of Power Sources* 196(1) (2011) 13-24.
- [10] E.S.R. Institute, What Are Lithium-Ion Batteries?, 2021.
- [11] P. Sideris, S. Greenbaum, Lithium Ion Batteries, *Electrochemical Reactions in*, 2013, pp. 239-283.
- [12] M. Li, J. Lu, Z. Chen, K. Amine, 30 Years of Lithium-Ion Batteries, *Advanced Materials* 30(33) (2018) 1800561.
- [13] J.B. Goodenough, Evolution of Strategies for Modern Rechargeable Batteries, *Accounts of Chemical Research* 46(5) (2013) 1053-1061.
- [14] B. Scrosati, History of lithium batteries, *Journal of Solid State Electrochemistry* 15(7) (2011) 1623-1630.
- [15] D.W. Murphy, J.N. Carides, Low Voltage Behavior of Lithium/Metal Dichalcogenide Topochemical Cells, *Journal of The Electrochemical Society* 126(3) (1979) 349.
- [16] M. Lazzari, B. Scrosati, A Cyclable Lithium Organic Electrolyte Cell Based on Two Intercalation Electrodes, *Journal of The Electrochemical Society* 127(3) (1980) 773.
- [17] J.J. Auborn, Y.L. Barberio, Lithium Intercalation Cells Without Metallic Lithium: and, *Journal of The Electrochemical Society* 134(3) (1987) 638.
- [18] T. Nagaura, Lithium ion rechargeable battery, *Progress in Batteries & Solar Cells* 9 (1990) 209.
- [19] K. Mizushima, P.C. Jones, P.J. Wiseman, J.B. Goodenough,  $\text{Li}_x\text{CoO}_2$  ( $0 < x \leq 1$ ): A new cathode material for batteries of high energy density, *Solid State Ionics* 3-4 (1981) 171-174.
- [20] Y. Huang, W. Li, J. Peng, Z. Wu, X. Li, X. Wang, Structure Design and Performance of the Graphite/Silicon/Carbon Nanotubes/Carbon (GSCC) Composite as the Anode of a Li-Ion Battery, *Energy & Fuels* 35(16) (2021) 13491-13498.

- [21] S. He, S. Huang, S. Wang, I. Mizota, X. Liu, X. Hou, Considering Critical Factors of Silicon/Graphite Anode Materials for Practical High-Energy Lithium-Ion Battery Applications, *Energy & Fuels* 35(2) (2021) 944-964.
- [22] E. Noh, R. Cong, J.-Y. Choi, Y. Hyun, H.-H. Park, M. Jo, H. Lee, C.-S. Lee, Synthesis, properties and electrochemical characteristics of SiNPs/CNT/rGO composite films for the anode material of Li ion batteries, *Applied Nanoscience* (2022).
- [23] B. Liang, Y. Liu, Y. Xu, Silicon-based materials as high capacity anodes for next generation lithium ion batteries, *Journal of Power Sources* 267 (2014) 469-490.
- [24] M.A. Rahman, G. Song, A.I. Bhatt, Y.C. Wong, C. Wen, Nanostructured Silicon Anodes for High-Performance Lithium-Ion Batteries, *Advanced Functional Materials* 26(5) (2016) 647-678.
- [25] M. Ashuri, Q. He, L.L. Shaw, Silicon as a potential anode material for Li-ion batteries: where size, geometry and structure matter, *Nanoscale* 8(1) (2016) 74-103.
- [26] X. Zuo, J. Zhu, P. Müller-Buschbaum, Y.-J. Cheng, Silicon based lithium-ion battery anodes: A chronicle perspective review, *Nano Energy* 31 (2017) 113-143.
- [27] T. Song, J. Xia, J.-H. Lee, D.H. Lee, M.-S. Kwon, J.-M. Choi, J. Wu, S.K. Doo, H. Chang, W.I. Park, D.S. Zang, H. Kim, Y. Huang, K.-C. Hwang, J.A. Rogers, U. Paik, Arrays of Sealed Silicon Nanotubes As Anodes for Lithium Ion Batteries, *Nano Letters* 10(5) (2010) 1710-1716.
- [28] M.-H. Park, M.G. Kim, J. Joo, K. Kim, J. Kim, S. Ahn, Y. Cui, J. Cho, Silicon Nanotube Battery Anodes, *Nano Letters* 9(11) (2009) 3844-3847.
- [29] S. Stankovich, D.A. Dikin, G.H.B. Dommett, K.M. Kohlhaas, E.J. Zimney, E.A. Stach, R.D. Piner, S.T. Nguyen, R.S. Ruoff, Graphene-based composite materials, *Nature* 442(7100) (2006) 282-286.
- [30] Y. Li, G. Xu, L. Xue, S. Zhang, Y. Yao, Y. Lu, O. Toprakci, X. Zhang, Enhanced Rate Capability by Employing Carbon Nanotube-Loaded Electrospun Si/C Composite Nanofibers As Binder-Free Anodes, *Journal of The Electrochemical Society* 160(3) (2013) A528.
- [31] L. Ji, X. Zhang, Evaluation of Si/carbon composite nanofiber-based insertion anodes for new-generation rechargeable lithium-ion batteries, *Energy & Environmental Science* 3(1) (2010) 124-129.
- [32] M.-S. Wang, W.-L. Song, J. Wang, L.-Z. Fan, Highly uniform silicon nanoparticle/porous carbon nanofiber hybrids towards free-standing high-performance anodes for lithium-ion batteries, *Carbon* 82 (2015) 337-345.
- [33] Y. Yan, H. Guo, Z. Wang, X. Li, G. Yan, J. Wang, Electrospinning-Enabled Si/C Nanofibers with Dual Modification as Anode Materials for High-Performance Lithium-Ion Batteries, *Acta Metallurgica Sinica (English Letters)* 34(3) (2021) 329-336.
- [34] T.J. Mason, Sonochemistry: Uses of Ultrasound in Chemistry and Related Disciplines, in: R.J. Siegel (Ed.), *Ultrasound Angioplasty*, Springer US, Boston, MA, 1996, pp. 25-54.
- [35] L. Zhang, A. Aboagye, A. Kelkar, C. Lai, H. Fong, A review: carbon nanofibers from electrospun polyacrylonitrile and their applications, *Journal of Materials Science* 49(2) (2014) 463-480.
- [36] D. Y, Y.N. Xia, Electrospinning of Nanofibers: Reinventing the Wheel?, *Advanced Materials* 16 (2004) 1151-1170.
- [37] K. Li, X. Ni, Q. Wu, C. Yuan, C. Li, D. Li, H. Chen, Y. Lv, A. Ju, Carbon-Based Fibers: Fabrication, Characterization and Application, *Advanced Fiber Materials* 4(4) (2022) 631-682.
- [38] S. Dalton, F. Heatley, P.M. Budd, Thermal stabilization of polyacrylonitrile fibres, *Polymer* 40(20) (1999) 5531-5543.

- [39] T.-H. Ko, Influence of continuous stabilization on the physical properties and microstructure of PAN-based carbon fibers, *Journal of Applied Polymer Science* 42(7) (1991) 1949-1957.
- [40] T.-H. Ko, The influence of pyrolysis on physical properties and microstructure of modified PAN fibers during carbonization, *Journal of Applied Polymer Science* 43(3) (1991) 589-600.
- [41] M.S.A. Rahaman, A.F. Ismail, A. Mustafa, A review of heat treatment on polyacrylonitrile fiber, *Polymer Degradation and Stability* 92(8) (2007) 1421-1432.
- [42] A. Smith, J. Burns, D. Xiong, J. Dahn, Interpreting high precision coulometry results on Li-ion cells, *Journal of The Electrochemical Society* 158(10) (2011) A1136.
- [43] B. Rumberg, B. Epling, I. Stradtmann, A. Kwade, Identification of Li ion battery cell aging mechanisms by half-cell and full-cell open-circuit-voltage characteristic analysis, *Journal of Energy Storage* 25 (2019) 100890.
- [44] X. Shen, Z. Tian, R. Fan, L. Shao, D. Zhang, G. Cao, L. Kou, Y. Bai, Research progress on silicon/carbon composite anode materials for lithium-ion battery, *Journal of Energy Chemistry* 27(4) (2018) 1067-1090.
- [45] J. McCarthy, S. Bhattacharya, T.S. Perova, R.A. Moore, H. Gamble, B.M. Armstrong, Composition and stress analysis in Si structures using micro-Raman spectroscopy, *Scanning* 26(5) (2004) 235-9.
- [46] W. Herres, J. Gronholz, Understanding FT-IR data processing, Part 1 (1984) 352-356.
- [47] A. Baravkar, R. Kale, S. Sawant, FTIR Spectroscopy: principle, technique and mathematics, *International Journal of Pharma and Bio Sciences* 2(1) (2011) 513-9.
- [48] M.S. Dresselhaus, G. Dresselhaus, R. Saito, A. Jorio, Raman spectroscopy of carbon nanotubes, *Physics Reports* 409(2) (2005) 47-99.
- [49] H.-C. Tao, L.-Z. Fan, Y. Mei, X. Qu, Self-supporting Si/Reduced Graphene Oxide nanocomposite films as anode for lithium ion batteries, *Electrochemistry Communications* 13(12) (2011) 1332-1335.
- [50] B. Shokri, M. Abbasi-Firouzjah, S.I. Hosseini, FTIR analysis of silicon dioxide thin film deposited by Metal organic-based PECVD, *Proceedings of 19th International Symposium on Plasma Chemistry Society* (2009).
- [51] E. Andrijanto, S. Shoelarta, G. Subiyanto, S. Rifki, Facile synthesis of graphene from graphite using ascorbic acid as reducing agent, 2016.
- [52] W. Lin, Y. Xiu, L. Zhu, K.-s. Moon, C.P. Wong, Assembling of carbon nanotube structures by chemical anchoring for packaging applications, 2008.
- [53] D. Alton, F. Heatley, M. Budd, Thermal stabilization of corresponding to preoxidation stages in DSC curves, polyacrylonitrile fibers, *Polymer* 40 (1999) 5531-5543.
- [54] Z. Wangxi, L. Jie, W. Gang, Evolution of structure and properties of PAN precursors during their conversion to carbon fibers, *Carbon* 41(14) (2003) 2805-2812.
- [55] T. Kim, W. Choi, H.-C. Shin, J.-Y. Choi, J.M. Kim, M.-S. Park, W.-S. Yoon, Applications of Voltammetry in Lithium Ion Battery Research, *J. Electrochem. Sci. Technol* 11(1) (2020) 14-25.
- [56] J. van Drunen, C. Locati, M. Kubicko, Electrochemical Battery Testing Methods Designed for Safety and Efficiency in a Research Laboratory, *ECS Meeting Abstracts MA2017-01(4)* (2017) 282.
- [57] X. Yang, A.L. Rogach, *Electrochemical Techniques in Battery Research: A Tutorial for Nonelectrochemists*, *Advanced Energy Materials* 9(25) (2019) 1900747.
- [58] F. Zhang, J. Yang, Boosting initial coulombic efficiency of Si-based anodes: a review, *Emergent Materials* 3(3) (2020) 369-380.

[59] X. Liu, X. Zhu, D. Pan, Solutions for the problems of silicon–carbon anode materials for lithium-ion batteries, *Royal Society Open Science* 5(6) (2018) 172370.